WARSAW UNIVERSITY OF TECHNOLOGY Index 351733
FACULTY OF CIVIL ENGINEERING
COMMITTEE FOR CIVIL AND WATER ENGINEERING
POLISH ACADEMY OF SCIENCES ISSN 1230-2945

DOI: 10.24425/ace.2023.145260

ARCHIVES OF CIVIL ENGINEERING

Vol. LXIX ISSUE 2 2023

pp. 165 –176

Research paper

Construction deviation control method of transverse super large inclined asphalt pavement

Yongzheng Qi[1, 2], Wengang Ma[3], Jiesheng Zhang[4]

Abstract: The speed of test vehicles on the high-speed car track of the automobile test field is very high. Reducing the construction error of asphalt pavement is very important to ensure the safety of the test vehicle. In order to realize the paving of asphalt concrete pavement with super-large lateral inclination in the curve section of the high-speed car track in the automobile test field, a special paving control device and control method for the construction on the curve section with super-large lateral inclination were developed. Use the direction of the hanging hammer under the GPS device of paver to adjust the position of GPS device in real time, so that the geometric centre line of GPS device is always perpendicular to the horizontal plane. The reference control line is preset in the paver operation control device, and the lateral displacement deviation of the paver is adjusted to synchronize the data of the paver control device with the travel route. The precise control of the paver's forward route is realized, the construction precision of the super-large inclined asphalt pavement on the high-speed car track of the automobile test field is achieved, and the construction efficiency is greatly improved. It has important reference value for similar projects such as automobile testing field and racing track.

Keywords: automobile testing ground, high-speed loop, super-large inclined road surface, asphalt pavement paving

[1]Prof., Yongzheng Qi, Key Laboratory of Flood & Drought Disaster Defense, the Ministry of Water Resources, Nanjing 210029, China, e-mail: zmxtree@just.edu.cn, ORCID: 0000-0001-8395-4552
[2]Prof., Yongzheng Qi, Jiangsu University of Science and Technology, School of Civil Engineering and Architecture, No. 2 Mengxi Road, Zhenjiang 212003, China, e-mail: zmxtree@just.edu.cn, ORCID: 0000-0001-8395-4552
[3]PhD., Wengang Ma, Institute of Civil Engineering and Intelligent Management, Nanjing Institute of Technology, Nanjing 211167, China, e-mail: morganseu@163.com, ORCID: 0000-0002-7807-1365
[4]Prof., Jiesheng Zhang, The First Engineering Co., LTD. of CTCE Group, No. 434 Fuyang North Road, Hefei 230041, China, e-mail: zjs980201@163.com, ORCID: 0000-0003-4296-7132

1. Introduction

The automobile test field is a special ground specially designed for testing the comprehensive performance of vehicles. Its high-speed loop test speed reaches more than 200 km/h. based on the consideration of vehicle driving safety, the construction error of high-speed loop pavement is highly required. The curve section of the high-speed car track in the test field of SAIC Volkswagen in Xinjiang adopts a super large inclined road with a maximum cross slope of 21% and an angle of 12°, as shown in Fig. 1 and Fig. 2. During the construction of the transverse inclined pavement of the curve section of the high-speed car track, the transverse horizontal deviation error of the paver has a great impact on the elevation error of the pavement, as shown in Figure 2. The relationship of pavement elevation error caused by horizontal deviation error is shown in formula (1.1).

$$\Delta x = \Delta y \tan 12^\circ \tag{1.1}$$

where, Δx is the elevation error of the pavement, and Δy is the horizontal offset value of the pavement. From the above formula, it can be seen that the asphalt pavement construction of the super large inclined pavement curve section of the high-speed car track in the automobile test field requires real-time adjustment of the travel route during the travel of the paver.

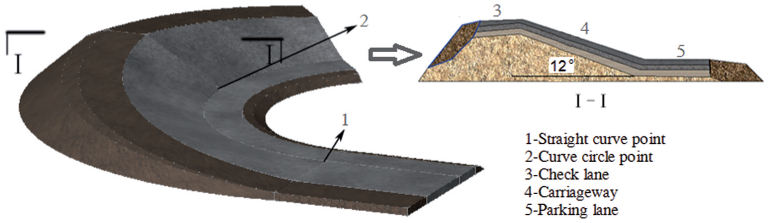

Fig. 1. Schematic diagram of curve segment model and section of high-speed loop

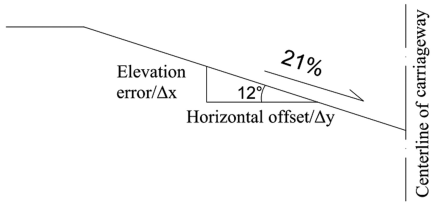

Fig. 2. Schematic diagram of pavement construction deviation

Shi et al. [1] aimed at the hysteresis characteristics of the screed for asphalt pavement curved paving, the phenomenon of excessive cross slope error often occurs in the superelevation section and the superelevation transition section. By analyzing the response characteristics of the screed under continuous step excitation, they determined the method of setting the parameters of the cross slope controller in curved paving, and proposed

the control method of curved paving. Zhu et al. [2] studied and developed an automatic control system for curve paving through the kinematic and dynamic models of variable slope paving. On the basis of finding the best start and end advance of slope change, the system automatically designs a control table of cross slope change value, which is input to the remote control interface of the cross slope controller of the paver as a control signal, so as to well control the error of the actual cross slope value and effectively improve the paving quality of the bend. Su et al. [3] used the weighted root mean square acceleration (RMSA) of the human body as the flatness evaluation index, and used CarSim software to establish the whole vehicle model and road model of the test vehicle to simulate the human vehicle road interaction. The field measurement evaluation method and simulation evaluation method of flatness were proposed. Zeng [4] introduced the information management concept of the Internet of things into pavement construction by using the pavement intelligent compaction monitoring system in the process of asphalt pavement construction. That provides real-time monitoring of the whole process during compaction and timely feedback the results. The quality control of pavement compaction process was realized. It provides a strong guarantee for improving the compaction quality of asphalt pavement. Gu et al. [5] adjusted the paving thickness, elevation, alignment and other parameters in real time through the control system installed on the paver to achieve the expected effect of dual control of pavement elevation and thickness. Wang et al. [6] designed a monitoring scheme based on the special design of optical fiberbased sensors to conduct the full-scale condition monitoring of asphalt pavements. Li et al. [7] used the finite element method (FEM) analysis and several professional commercial software to analyze the pavement structure, and established the field test section. The results show that the multi axle sandwich can improve the stress distribution more effectively than the double yarn double axle sandwich. Tutka et al. [8] studied discusses the effect of pavement displacement discontinuity on the observed deflection basin and compares the results with those for a model with continuity. Li [9] carried out research on improving the paving construction accuracy of small radius continuous sharp turn asphalt pavement. Comprehensive analysis was carried out from the aspects of paving equipment, square finding type, feeding mode, paving speed and rolling combination. A complete set of construction technology for small radius continuous sharp turn asphalt pavement construction was summarized. The construction quality was improved and the construction cost is reduced. Wang [10] used the dynamic quality monitoring system to pave the asphalt concrete pavement, and dynamically collected and analyzed the application data generated in the construction process. The application data could be monitored all-weather by information method, and the paving uniformity of asphalt concrete pavement and the compaction characteristics of pavement base could be controlled in real time. The author studied the application of intelligence in the construction of asphalt concrete pavement, and carried out reasonable and quantitative quality control in the construction process. The uniformity of paving and compactness of pavement are further improved. Horan et al. [11] described how to use integrated circuit technology as a valuable tool to improve the quality control of HMA project. These new integrated circuit tools include on-board color coding display, which can measure the underlying material support before paving, and collect data for statistical analysis of

the effectiveness of compaction operation. Lei et al. [12] studied the 3D paving control technology of asphalt concrete pavement, which realizes the purpose of high-precision paving of asphalt mixture. Li et al. [13] used the self-developed laser profiler to collect the spatial coordinates of the measuring points, adopted the concept of small spacing and multi line measurement, and used the MATLAB software platform to process the measured data to realize the three-dimensional reconstruction of asphalt pavement. Fu et al. [14] developed an intelligent asphalt pavement paving thickness control system using a single host, multi-channel ground penetrating radar system. It realized high-precision real-time monitoring, analysis and display of asphalt pavement paving thickness. The evaluation method of pavement paving thickness was established based on the discrete index of loose paving thickness, the standard rate of paving thickness and the thickness cost control rate. Wang [15] applied the intelligent monitoring system to the asphalt pavement paving construction. According to the operation characteristics of the paver, it was equipped with a global navigation satellite system whose recognition accuracy was centimeter level, which monitors and counts the asphalt mixture paving mileage and paving speed. The dual capture of paving trajectory and positioning was completed by using real-time dynamic difference technology. Yu et al. [16] used three-dimensional ground penetrating radar technology to scan the full section of asphalt pavement. By collecting the pavement thickness distribution data matrix and drawing the thickness distribution cloud map, the dynamic adjustment of the upper paving construction was carried out. The qualified rate of pavement thickness was effectively improved, and the uniformity of thickness distribution was greatly improved. Danoshini et al. [17] 14assessed the mechanical performance of stone mastic asphalt incorporating kenaf fibre by developing a regression model. Baqadeem et al. [18] discussed some main properties of asphalt mixture, such as stability and flow. The research displayed that using glass waste in asphalt mixture is acceptable. Shahnewaz et al. [19] discussed the overall performance and advantage of porous asphalt using different types of additives. Al- Saffar et al. [20] explored the performance and durability of rejuvenated asphalt mixtures embedded with several types of rejuvenators identified from the extensive literature review. Aletba et al. [21] provides a detailed review of the thermal properties of these mitigation measures in the context of cool asphalt pavements. Zhang et al. [22] realized the fast and intelligent positioning and setting out of tunnel excavation face. This research is aimed to achieve the construction precision of the super-large inclined asphalt pavement without horizontal deviation on the high-speed car track of the automobile test field.

2. Paving control system of transverse super inclined asphalt pavement of high-speed car track

When the paver paves on the transverse super large inclined asphalt pavement of the high-speed car track, the gravity direction of the hammer installed under the GPS is used to adjust the position of the GPS device in real time, so that the geometric center line of

the GPS device is always perpendicular to a horizontal plane. Preset the reference control line in the paver forward control device, and adjust the horizontal and horizontal deviation of the paver according to the reference control line, so that the real-time detection data of the paver control device is synchronized with the paver forward route, as shown in Fig. 3.

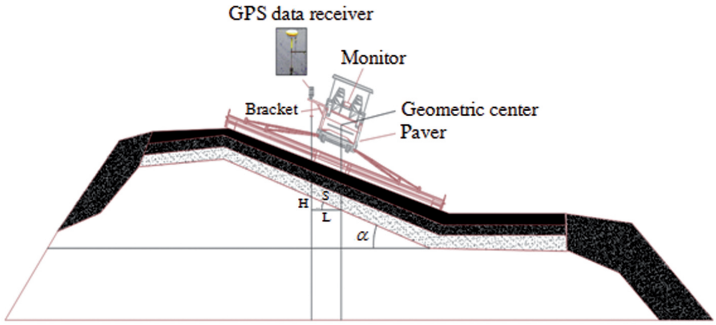

Fig. 3. Schematic diagram of gravity GPS paving control system for laterally inclined pavement

Where, α is the included angle between the transverse inclined road surface of the high-speed car track and the horizontal line, L is the distance between the projection point in the direction of the plumb line measured by the GPS signal receiver and the projection point of the geometric centroid of the paver, S is the distance between the GPS plumb projection point to be controlled and the reference control line of the paver, and H is the vertical distance from the projection point of the road surface of the plumb to the projection point of the geometric center. Firstly, the S value that should be controlled by each paving point is calculated through the given longitudinal and transverse slopes of each curve section of the high-speed car track in the automobile test field. Then all the data are input into the program to realize the real-time control in the process of asphalt pavement paving.

Assuming cross slope $i = H/L = \tan\alpha$, then $\alpha = \arctan i$ we get

$$L = S \cdot \cos\alpha = S \cdot \cos(\arctan i), \qquad H = S \cdot \cos\alpha = S \cdot \cos(\arctan i) \tag{2.1}$$

It can be seen that there is a correlation between the GPS vertical projection point and the geometric centroid projection point of the paver during the paving process. Using this correlation can ensure the accuracy of asphalt concrete pavement paving construction.

First, the plane position (x_i, y_i) of the paver is obtained by GPS. The mileage k_i of the design route corresponding to the paver at this moment is calculated by the compiled program. Then, the section inclination α_i corresponding to the current mileage position and the horizontal distance l_i between the GPS vertical projection point and the line center are calculated. Finally, the deviation value to guide the paver construction will be adjusted.

In order to realize the real-time positioning of the measurement points of the paving control panel, it is necessary to convert the GPS coordinates through the coordinates of the midpoint of the curve, as shown in Fig. 4. Where, point O is the starting point of the spiral,

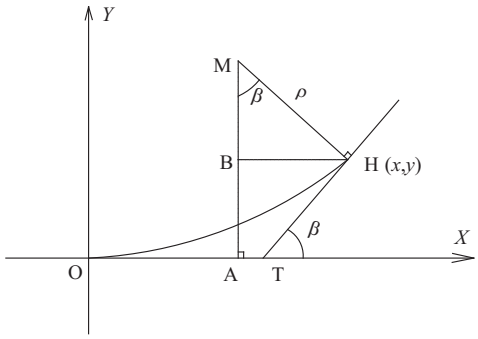

Fig. 4. Calculation of transition curve coordinate points

OX is the tangent, c is the spiral constant ($c = R \cdot s$, R is the radius of the circular curve, s is the length of the spiral), and ρ = MH is the distance from point M to the spiral. Then

$$\rho = \frac{s^2}{2c} \tag{2.2}$$

The tangent of the transition curve passing through point h intersects OX at point T. ρ = MH is the distance from point M to the transition curve (MH $\perp$ HT), and the vertical line of OX passing through point M intersects OX at point A. Then $\beta = \angle\text{XTH} = \angle\text{AMH}$.

Let it be the length of the transition curve from point O to point h, then the rectangular coordinate value (x, y) of the perpendicular foot can be calculated by equation (2.3)

$$\begin{cases} x = \displaystyle\int_0^s \cos\beta(s)\,\mathrm{d}s = s - \frac{s^5}{40c^2} + \frac{s^9}{3456c^4} - \frac{s^{13}}{599040c^6} + \cdots \\ y = \displaystyle\int_0^s \sin\beta(s)\,\mathrm{d}s = \frac{s^3}{6c} - \frac{s^7}{336c^3} + \frac{s^{11}}{42240c^5} - \frac{s^{15}}{9676800c^7} + \cdots \end{cases} \tag{2.3}$$

From the relationship of right triangle MHB, we get

$$\begin{cases} x - x_0 = (y_0 - y)\tan\beta \\ \beta = (y_0 - y)\sec\beta \end{cases} \qquad \left(0 \le \beta < \frac{\pi}{2}\right) \tag{2.4}$$

By polynomial transformation formula

$$\begin{cases} \tan\beta = \tan\dfrac{s^2}{2c} = \dfrac{s^2}{2c} + \dfrac{s^6}{24c^3} + \dfrac{s^{10}}{240c^5} + \cdots \\ \sec\beta = \sec\dfrac{s^2}{2c} = 1 + \dfrac{s^4}{8c^2} + \dfrac{5s^8}{384c^4} + \cdots \end{cases} \tag{2.5}$$

Substituting formula (2.3) and formula (2.5) into formula (2.4), we get

$$\begin{cases} s = x_0 + \phi(s) \\ \rho(s) = y_0\left(1 + \dfrac{s^4}{8c^2} + \dfrac{5s^8}{384c^4} + \cdots\right) - \left(\dfrac{s^3}{6c} + \dfrac{s^7}{56c^3} + \dfrac{101s^{11}}{55440c^5} + \cdots\right) \end{cases} \tag{2.6}$$

where

$$\phi(s) = y_0\left(\frac{s^2}{2c} + \frac{s^6}{24c^3} + \frac{s^{10}}{240c^5} + \cdots\right) - \left(\frac{7s^5}{120c^2} + \frac{139s^9}{24192c^4} + \cdots\right) \tag{2.7}$$

By Lagrange expansion theorem

$$\rho(s) = \rho(x_0) + \sum_{n=1}^{\infty} \frac{1}{n!} \frac{\partial^{n-1}}{\partial x_0^{n-1}} \left[\rho'(x_0)\phi''(x_0)\right] \tag{2.8}$$

Then

$$\rho(x_0) = y_0\left(1 + \frac{x_0^4}{8c^2} + \frac{5x_0^8}{384c^4} + \cdots\right) - \left(\frac{x_0^3}{6c} + \frac{x_0^7}{56c^3} + \frac{101x_0^{11}}{55440c^5} + \cdots\right) \tag{2.9}$$

$$\rho'(x_0) = y_0\left(\frac{x_0^3}{2c^2} + \frac{5x_0^7}{48c^4} + \cdots\right) - \left(\frac{x_0^2}{2c} + \frac{x_0^6}{8c^3} + \frac{101x_0^{10}}{5040c^5} + \cdots\right) \tag{2.10}$$

$$\phi(x_0) = y_0\left(\frac{x_0^2}{2c} + \frac{x_0^6}{24c^3} + \frac{x_0^{10}}{240c^5} + \cdots\right) - \left(\frac{7x_0^5}{120c^2} + \frac{139x_0^9}{24192c^4} + \cdots\right) \tag{2.11}$$

Find the value of ρ'', substitute them into equation (2.11), we get

$$\rho = \left(-\frac{x_0^3}{6c} + \frac{19x_0^7}{1680c^3} - \frac{24823x_0^{11}}{13305600c^5} + \cdots\right) + y_0\left(1 - \frac{x_0^4}{8c^2} + \frac{61x_0^8}{1920c^4} - \cdots\right) - y_0^2\left(\frac{x_0^5}{8c^3} - \frac{13x_0^9}{192c^5} + \cdots\right) - y_0^3\left(\frac{x_0^6}{48c^4} - \cdots\right) \tag{2.12}$$

Take the first four terms of the polynomial and get

$$\rho = y_0 - \frac{x_0^3}{6c} - \frac{y_0 x_0^4}{8c^2} - \frac{19x_0^7}{1680c^3} \tag{2.13}$$

When point M is on the upper side of the spiral, it is positive; on the lower side of the spiral, it is negative; and on the spiral, it is zero.

Thus, the coordinate formula of the vertical foot H (x,y) can be obtained as

$$\begin{cases} x = x_0 + \dfrac{x_0^2 y_0}{2c} + \left(-\dfrac{x_0^5}{12} + \dfrac{x_0^3 y_0^2}{2}\right)\dfrac{1}{c^2} - \dfrac{9x_0^6 y_0}{40c^3} \\ y = \dfrac{x_0^3}{6c} + \dfrac{x_0^4 y_0}{4c^2} - \dfrac{9x_0^7}{280c^3} \end{cases} \tag{2.14}$$

The distance from point m to the transition curve can be calculated directly by formula (2.13). You can also calculate the distance from the point to the perpendicular point after obtaining the coordinates of the perpendicular foot through formula (2.14).

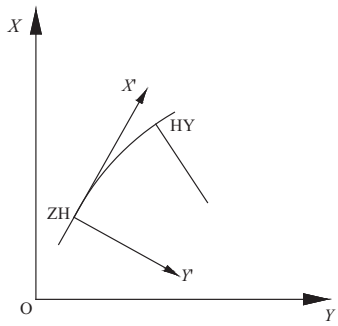

Fig. 5. Schematic diagram of local coordinate system

In order to list the error calculation equation in the transition curve segment, coordinate conversion is required. Set the tangent of the straight and gentle point as the X' axis and the vertical line of the tangent as the Y' axis to establish the local coordinate system, as shown in Fig. 5.

Take the tangent right deviation of the spiral relative to the ZH point as an example.

$$\begin{pmatrix} x_i \\ y_i \end{pmatrix} = \begin{pmatrix} x_{zh} \\ y_{zh} \end{pmatrix} + \begin{pmatrix} \cos\alpha & -\sin\alpha \\ \sin\alpha & \cos\alpha \end{pmatrix} \begin{pmatrix} x_i' \\ y_i' \end{pmatrix} \tag{2.15}$$

where, α is the azimuth of the tangent of ZH point in the external coordinate system.

In the local coordinate system, the relationship between the transition curve length s_0 and the turning angle β_i at the coordinates (x_i', y') and i of the transition curve point a is as follows

In the local coordinate system, the relationship between the coordinates (x_i', y') of spiral point i, the turning angle β_i at point i and the spiral length s is as follows

$$\begin{cases} x_i' = s_i - \dfrac{s_i^5}{40R^2 s_0^2} + \dfrac{s_i^9}{3456R^4 s_i^4} - \cdots \\ y_i' = \dfrac{s_i^3}{6Rs_0} - \dfrac{s_i^7}{336R^3 s_0^3} + \dfrac{s_i^{11}}{42240R^5 s_0^5} - \cdots \\ \beta_i = \dfrac{s_i^2}{2Rs_0} \end{cases} \tag{2.16}$$

where, s_i is the length of the transition curve at point i, R is the radius of the curve segment, and s_0 is the total length of the transition curve segment.

According to formula (2.15), we can get

$$\begin{cases} x_i = x_{zh} + x_i' \cos\alpha - y_i' \sin\alpha \\ y_i = y_{zh} + x_i' \sin\alpha + y_i' \cos\alpha \end{cases} \tag{2.17}$$

Differential s_i on both sides of equation (2.17) to obtain the deviation calculation equation (2.18)

$$\begin{cases} v_{x_i} = \delta x_{zh} + \cos(\alpha - \beta_i) ds_i + a_{xk}\delta k + a_{xR}\delta R + a_{xs_0}\delta s_0 - \left(x_i - x_i^0\right) \\ v_{y_i} = \delta y_{zh} + \sin(\alpha - \beta_i) ds_i + a_{yk}\delta k + a_{yR}\delta R + a_{ys_0}\delta s_0 - \left(y_i - y_i^0\right) \end{cases} \tag{2.18}$$

Keeping the total length of the transition curve unchanged, we get

$$\begin{cases} v_{x_i} = \delta x_{zh} + \cos(\alpha - \beta_i) ds_i + a_{xk}\delta k + a_{xR}\delta R - \left(x_i - x_i^0\right) \\ v_{y_i} = \delta y_{zh} + \sin(\alpha - \beta_i) ds_i + a_{yk}\delta k + a_{yR}\delta R - \left(y_i - y_i^0\right) \end{cases} \tag{2.19}$$

where

$$a_{xk} = \left(-x_i'^0 \sin\alpha^0 - y_i'^0 \cos\alpha^0\right) \cos^2(\alpha^0) \tag{2.20}$$

$$a_{yk} = \left(x_i'^0 \cos\alpha^0 - y_i'^0 \sin\alpha^0\right) \cos^2(\alpha^0) \tag{2.21}$$

$\delta\alpha = \cos^2(\alpha^0)\delta k$, k is the slope of the straight line segment

$$\begin{pmatrix} a_{xR} & a_{xs_0} \\ a_{yR} & a_{ys_0} \end{pmatrix} = \begin{pmatrix} \cos\alpha^0 & -\sin\alpha^0 \\ \sin\alpha^0 & \cos\alpha^0 \end{pmatrix} \begin{pmatrix} a'_{xR} & a'_{xs_0} \\ a'_{yR} & a'_{ys_0} \end{pmatrix} \tag{2.22}$$

$$a'_{xR} = \frac{s_i^5}{20R^3 s_0^2} - \frac{s_i^9}{864R^5 s_0^4} \tag{2.23}$$

$$a'_{yR} = -\frac{s_i^3}{6R^2 s_0} + \frac{s_i^7}{112R^4 s_0^3} - \frac{s_i^{11}}{8448R^6 s_0^5} \tag{2.24}$$

$$a'_{xs_0} = \frac{R}{s_0} a'_{xR} \tag{2.25}$$

$$a'_{ys_0} = \frac{R}{s_0} a'_{yR} \tag{2.26}$$

The key of the paver travel control device is to ensure that the gravity GPS real-time monitoring system must remain vertical at any time. The gravity GPS control device developed is composed of GPS real-time monitor, displacement flat panel display, steel pipe support, movable ring, gravity hanging hammer and connecting rod, as shown in Fig. 6. Two wedge blocks are set in the device. The top of the wedge block is designed as an isosceles triangular slope, so that the top of the wedge block contacts the groove of the steel pipe support. The friction between the movable ring and the groove is reduced to ensure that the gravity GPS real-time monitoring system remains vertical together with the movable ring.

The display device in the construction control device of the paver is placed in the cab of the paver, and the steel pipe support is installed on the side of the cab of the paver, as shown in Fig. 7.

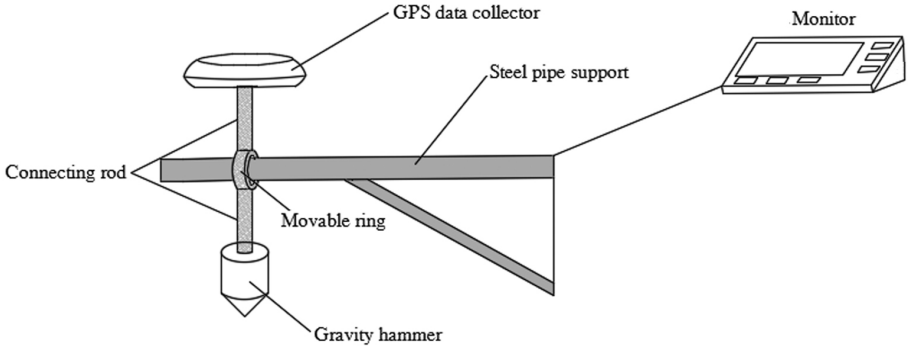

Fig. 6. Schematic diagram of gravity GPS real-time monitoring system

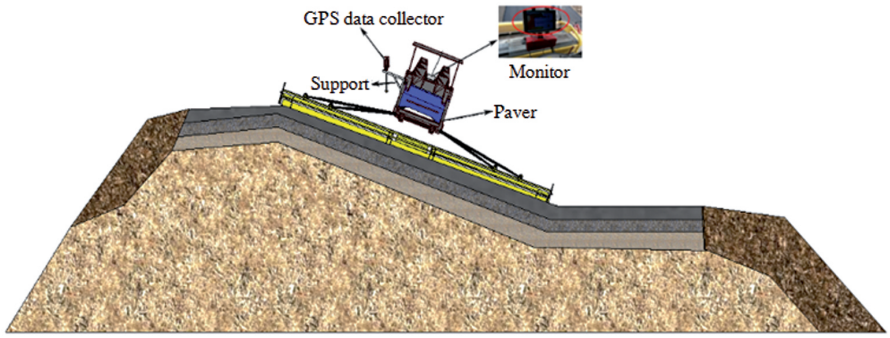

Fig. 7. Schematic diagram of paver GPS real-time monitoring device

3. Application examples

Xinjiang SAIC Volkswagen testing ground is the first automobile testing ground built in dry and hot, desert climate and strong saline soil areas in China. Its high-speed loop length is 13 km, of which the length of the curve section is 9.9 km. The loop length and the scale of the testing ground are in the forefront of similar projects in the world. The transverse super large inclined asphalt pavement of the high-speed car track is composed of broken lines, with a maximum cross slope of 21%.

In the construction process, gravity GPS guiding device and paver real-time monitoring system are adopted. By calculating the equation for the deviation, the horizontal deviation is adjusted in real time, and each construction index is refined. Through the collection and sorting of construction data, intellectualization, so that the paving operation of high-speed car track asphalt pavement can be guided. The measured IRI (International evenness index) of the asphalt pavement evenness of the high-speed car track in the post construction three-dimensional laser scanning test field is 0.6~0.8 m/km, which is far less than the design requirement of 1.5 m/km. The qualified rate is 100%.

4. Conclusions

Asphalt pavement paving in the curved section of the inclined pavement of the high-speed car track was the construction difficulty of the project. Through a series of theoretical derivation, the deviation calculation equation is obtained. By setting up a special control device and adopting a gravity GPS real-time monitoring system, the problem of controlling the paving benchmark of different transverse inclined roads on the high-speed car track in the testing ground was solved. The construction accuracy was far less than the design requirements, which greatly improves the construction efficiency and achieves good economic and social benefits. This method has a broad application prospect in similar projects such as automobile test field and race track.

Acknowledgements

This work is supported by the Open Fund of Key Laboratory of Flood & Drought Disaster Defense, the Ministry of Water Resources (Grant No. KYFB202112071029), and the Scientific Research Foundation for the High-level Personnel of Nanjing Institute of Technology (Grant No. YKJ201984).

References

[1] W. Shi, H. Zhang, and M. Li, "The Parameters Setting of Transverse Slope Controller Paving in Curve Paving of Asphalt Pavement", *Equipment Manufacturing Technology*, no. 3, pp. 155–156, 2014, doi: 10.3969/j.issn.1672-545X.2014.03.056.

[2] M.C. Zhu and Z.X. Luan, "Study on Auto-control System of Varying Grade Paving", *Construction Machinery & Construction Technology*, vol. 27, no. 9, pp. 45–47, 2010, doi: 10.3969/j.issn.1000-033X.2010.09.020.

[3] M.M. Su and H.L. Zhang, "Evaluation method of asphalt pavement roughness based on full car model", *Journal of Jiangsu University (Natural Science Edition)*, vol. 38, no. 3, pp. 361–366, 2017, doi: 10.3969/j.issn.1671-7775.2017.03.019.

[4] Q.C. Zeng, "Application of Road Surface Intelligent Compaction Monitoring System in Asphalt Pavement Construction of Yunzhan Expressway", *Technology of Highway and Transport*, vol. 34, no. 4, pp. 21–25, 2018, doi: 10.13607/j.cnki.gljt.2018.04.005.

[5] J.M. Gu, W.J. Zou, W.H. Bai, et al., "Application of 3D Intelligent Digital Paving Technology in Pavement Construction of Li-Gao Expressway", *Construction Quality*, vol. 39, no. 2, pp. 65–68, 2021, doi: 10.3969/j.issn.1671-3702.2021.02.016.

[6] H.P. Wang, P. Xiang, and Z. Jiang, "Optical fiber sensing technology for full-scale condition monitoring of pavement layers", *Road Materials and Pavement Design*, vol. 21, no. 5, pp. 1258–1273, 2020, doi: 10.1080/14680629.2018.1547656.

[7] P. Li, J. Liu, and S. Zhao, "Performance of Multiaxial Paving Interlayer–Reinforced Asphalt Pavement", *Journal of Materials in Civil Engineering*, vol. 28, no. 7, pp. 1–9, 2016, doi: 10.1061/(ASCE)MT.1943-5533.0001543.

[8] P. Tutka, R. Nagórski, and M. Złotowska, "Backcalculation of flexible pavement moduli including interlayer bonding conditions–numerical analysis", *Archives of Civil Engineering*, vol. 68, no. 3, pp. 5–22, 2022, doi: 10.24425/ace.2022.141870.

[9] G. Li, "Study on the optimization method of improving the paving construction accuracy of small radius continuous sharp turn asphalt pavement", *Engineering and Technological Research*, vol. 4, no. 8, pp. 205–207, 2019, doi: 10.19537/j.cnki.2096-2789.2019.08.095.

[10] W.H. Wang, "Application of intelligence in asphalt concrete pavement paving and base compaction", *TranspoWorld*, no. 7, 205-207, pp. 58–59, 2022, doi: 10.16248/j.cnki.11-3723/u.2022.07.018.

[11] R.D. Horan, G.K. Chang, Q. Xu, et al., "Improving Quality Control of Hot-Mix Asphalt Paving with Intelligent Compaction Technology", *Transportation Research Record: Journal of the Transportation Research Board*, vol. 2268, no. 1, pp. 82–91, 2012, doi: 10.3141/2268-10.

[12] X.L. Lei and G. Li, "Applied Research of 3D Paving Control Technology in Asphalt Pavement Works", *Journal of Municipal Technology*, vol. 36, no. 5, pp. 20–24, 2018.

[13] Z. Li, J. Liu, and G.Y. Su, "Three-dimension Reconstruction of Asphalt Pavement Contour Features Based on Laser Profiler", *Highway Engineering*, vol. 44, no. 5, pp. 47–52, 2019, doi: 10.19782/j.cnki.1674-0610.2019.05.010.

[14] L.R. Fu, J.P. Huang, M.J. Liao, et al., "Research on asphalt pavement paving thickness and pavement 3D visualization technology based on ground penetrating radar", *Highways & Automotive Applications*, no. 3, pp. 76–79+85, 2022, doi: 10.20035/j.issn.1671-2668.2022.03.019.

[15] S.G. Wang, "Application of intelligent monitoring system in asphalt pavement paving construction", *China High and New Technology*, no. 24, pp. 72–73, 2021, doi: 10.13535/j.cnki.10-1507/n.2021.24.32.

[16] J.M. Yu, T.J. Ming, X.N. Zhang, et al., "Research on dynamic adjustment technology of asphalt pavement thickness based on three-dimensional ground penetrating radar", *Journal of China & Foreign Highway*, vol. 40, no. 3, pp. 70–75, 2020, doi: 10.14048/j.issn.1671-2579.2020.03.015.

[17] G. Danoshini, A. Baqadeem, A.K.S. Al-Shakhrit, et al., "Statistical Analysis of Stone Mastic Asphalt Incorporating Kenaf Fibre", *Construction*, vol. 1, no. 1, pp. 12–17, 2021, doi: 10.15282/construction.v1i1.6282.

[18] B.A.O. Abdullah, F.M. Jakarni, A.K.S. Al-Shakhrit, et al., "The usage of Recycled Glass In Hot Mix Asphalt: A Review", *Construction*, vol. 1, no. 1, pp. 29–34, 2021, doi: 10.15282/construction.v1i1.6324.

[19] S.M. Shahnewaz, K.A. Masri, and N. Ghani, "Porous Asphalt Modification using Different Types of Additives: A Review", *Construction*, vol. 1, no. 1, pp. 44–53, 2021, doi: 10.15282/construction.v1i1.6502.

[20] Z.H. Al-Saffar, H. Yaacob, H.Y. Katman, et al., "A Review on the Durability of Recycled Asphalt Mixtures Embraced with Rejuvenators", *Sustainability*, vol. 13, no. 16, pp. 1–24, 2021, doi: 10.3390/su13168970.

[21] S.R.O. Aletba, N.A. Hassan, R.P. Jaya, et al., "Thermal performance of cooling strategies for asphalt pavement: a state-of-the-art review", *Journal of Traffic and Transportation Engineering (English Edition)*, vol. 8, no. 3, pp. 356–373, 2021, doi: 10.1016/j.jtte.2021.02.001.

[22] J.S. Zhang and Y.Z. Qi, "Research on the intelligent positioning method of tunnel excavation face", *Archives of Civil Engineering*, vol. 68, no. 1, pp. 431–441, 2022, doi: 10.24425/ace.2022.140178.

Received: 2022-07-22, Revised: 2022-10-25